PHOTOOXIDATION OF ARYL PHOSPHINES IN METAL ORGANIC FRAMEWORKS: A MECHANISTIC PROBE FOR CAGE EFFECTS

A Thesis

Presented to

The Faculty of the Department of Chemistry and Biochemistry

California State University, Los Angeles

In Partial Fulfillment

of the Requirements for the Degree

Master of Science

in

Chemistry

By

Nicole Caye Rearo Salimbangon

December 2024

© 2024

Nicole Caye Reario Salimbangon

ALL RIGHTS RESERVED

The thesis of Nicole Caye Reario Salimbangon is approved.

Matthias Selke, Ph.D., Committee Chair

Yangyang Liu, Ph.D.

Brenda Andrade Rounds, Ph.D.

Olaseni Sode, Ph.D.

California State University, Los Angeles

December 2024

ABSTRACT

The Photooxidation of Aryl Phosphines in Metal-Organic Frameworks: A Mechanistic Probe for Cage Effects

By

Nicole Caye Rearo Salimbangon

Arylphosphines are a class of organophosphorus compounds widely used in catalysis and polymerization and as jet fuel stabilizers. The bulkiness of these compounds can be modified with substituents on the ortho position of the aryl group. Many arylphosphines are inert and, therefore, unreactive with triplet oxygen. In contrast, they react readily with singlet oxygen, leading to phosphine oxides and/or phosphinate esters. The ratio of these products is susceptible to steric effects: the intramolecular formation of the phosphinate ester is preferred in a sterically demanding environment. This research studied the reactivity change of phosphine oxidation chemistry inside metal-organic frameworks (MOFs). We used the photooxidation of triphenylphosphine and tris(ortho-methoxyphenyl) phosphine as the substrates and MOFs with porphyrin linkers as the photocatalyst. If the reactions occurred inside the MOF pores, rearrangement to phosphinate ester should be preferred since phosphine oxide formation requires intermolecular oxygen atom transfer from the phosphadioxirane intermediate to a second molecule of triarylphosphine.

In contrast, the rearrangement of the phosphadioxirane to the phosphinate ester is a unimolecular process. Other MOFs with varying pore sizes were also examined for

their cage effects. We have found no increase in the phosphinate ester product relative to homogeneous solution phase chemistry. This result implies that singlet oxygen diffuses out of the MOF cage, and the photooxidation with phosphines occurs outside the cage, in contrast to previous suggestions in the literature. However, there are traces of the insertion product formation in the photooxidation of triphenylphosphine in PCN-222. We have also investigated the rate of triphenylphosphine oxidation in PCN-222 vs the rate of photooxidation of 9,10-dimethylanthracene (DMA). We determined that the rate constant ratio of 3.4 for the two MOF-catalyzed reactions is very close to the rate constant ratio of 4.0 in a homogeneous solution. Since the relative reactivity of DMA and phosphine towards singlet oxygen remains consistent between homogeneous solution and the PCN-222-catalyzed reactions, it is likely that DMA predominantly interacts with singlet oxygen molecules that have diffused out of the MOF pores. We also found that the reaction of the triphenylphosphine with singlet oxygen only takes place outside the MOF due to the more significant steric requirements of the MOF. In general, evaluating such relative rate constant ratios may provide a method to assess whether singlet oxygen reactions occur inside and/or outside of the MOF pores.

ACKNOWLEDGMENTS

I would like to express my sincere gratitude to Dr. Selke Matthias, my primary research advisor, for this invaluable guidance, unwavering support, and mentorship throughout this research project. I also acknowledge my co-advisor, Dr. Liu, for her encouragement, insightful feedback, and valuable contributions.

I am deeply grateful to my committee members, Dr. Brenda Andrade Rounds and Dr. Olaseni Sode, for their insightful feedback, constructive criticism, and support. Their valuable perspectives have significantly enriched this research.

I would also like to thank my lab mates in Dr. Selke's and Dr. Liu's lab, for their assistance, collaboration, and creating a supportive and stimulating research environment. I am grateful for their helpful discussions, technical assistance, and camaraderie.

I extend my heartfelt thanks to my family and friends for their unwavering support and encouragement throughout my graduate studies. Their belief in me and their constant support has been imperative.

Finally, I would like to acknowledge the financial support provided by NSF HRD-2112554, which made this research possible.

TABLE OF CONTENTS

Abstract iv

Acknowledgments v

List of Tables viii

List of Figures ix

Chapter

1. Singlet Oxygen: Generation, Reactivity, and Interactions with Aryl Phosphines ..1

2. Porphyrin-Based Metal-Organic Frameworks 10

3. Metal-Organic Frameworks (MOFs): Synthesis and Characterization 13

3.1 Materials 13

3.2 Instrumentation 13

3.3 Synthesis of Al-TCPP 13

3.4 Synthesis of PCN-222 14

3.5 Characterization of MOFs 15

4. Photooxidation of Arylphosphines and 9,10 Dimethyl anthracene in Porphyrin and MOFs: Results 17

4.1 Materials 17

4.2 Photooxidation Reactions with MOFs 17

4.2.1. General Procedure for the Photooxidation of Arylphosphines in Porphyrin and Porphyrin-based MOF 17

4.2.2. General Procedure for the Photooxidation of 9,10-Dimethylanthracene in Porphyrin and Porphyrin based MOFs 18

4.3 Results.....18

4.3.1 Photooxidation of Tris(ortho-methoxyphenyl) phosphine Al-TCPP.....18

4.3.2 Photooxidation of Tris(ortho-methoxyphenyl) phosphine in PCN-222.....20

4.3.3 Photooxidation of Triphenylphosphine (TPP) with Meso-tetra(4-carboxyphenyl) porphyrin and PCN-222.....24

4.4 Comparison of Relative Rate Constants for Photooxidation of Triphenyl Phosphine in PCN-222 and Homogenous Solution with Rate Constants for Photooxidation of 9,10-Dimethylanthracene (DMA) Catalyzed by PCN 222 and in Homogeneous Solution.....27

4.4.1 Photooxidation of 9,10 Dimethyl anthracene with PCN-222.....28

4.4.2 Rate of Disappearance Analysis and Comparison of Rate Constants of 9,10 Dimethylanthracene and Triphenylphosphine with PCN-222.....29

5. Concluding Remarks and Directions for Future Research.....32

References.....33

LIST OF TABLES

Table

1. Integration of ^{31}P NMR peaks from Figure 12 of the product and starting material ratios with respect to time in minutes 21
2. Integration of ^{31}P NMR peaks from Figure 13 of the product and starting material ratios with respect to time in minutes 22
3. Integration of ^{31}P NMR peaks from Figure 15 of the product and starting material ratios with respect to time in minutes 23
4. Integration of ^{31}P NMR peaks Integral values from Figure 16 of the product and starting material ratios with respect to time in minutes 25
5. Integration of ^{31}P NMR Peaks from Figure 17 of the product and starting material ratios with respect to time in minutes 27
6. Integral values from Figure 19 of the product (DMA-O_2) and starting material (DMA) ratios with respect to time in minutes 28

LIST OF FIGURES

Figure

1. Modified Molecular Orbital Diagram of $^1O_2$ and $^3O_2$.....2
2. Singlet oxygen pathway via photosensitization with Type 1 and Type 2 mechanisms and products 3
3. Representative scheme of electrophilic oxidative addition reactions of nucleophiles with singlet oxygen: (a) singlet oxygen ene reaction; (b) [2+2 cycloaddition; (c) [4+2] cycloaddition; (d) photooxidation of sulfides; (e) photooxidation of aryl phosphines.....4
4. Scheme of singlet oxygen reaction with 9,10 dimethyl anthracene.....5
5. Space-filling model of Tolman's cone angle 6
6. Reaction of singlet oxygen with *ortho*-substituted arylphosphines in a homogeneous media proceeding different pathways yielding two varying products.....7
7. Detailed mechanism of singlet oxygen reaction with tris (ortho-methoxyphenyl) phosphine. 8
8. A three-dimensional model of a MOF structure 11
9. Model Scheme of a MOF cage confining tris(ortho methoxyphenyl) phosphine .12
10. A reaction scheme for synthesizing PCN-222 with zirconium as the metal salt and TCPP as the organic linker. 15
11. Al-TCPP MOF Powder X-ray Diffraction (PXRD), Nitrogen Adsorption/ Desorption Isotherm (N_2 Isotherm) Analysis, and DFT Pore Distribution.....16

12. PCN-222 MOF Powder X-ray Diffraction Pattern (PXRD), Nitrogen Adsorption/ Desorption Isotherm (N_2 Isotherm) Analysis, and DFT Pore Distribution.....16

13. ^{31}PNMR data spectra analysis of tris(ortho-methoxyphenyl) phosphine with Meso-tetra(4-carboxyphenyl) porphyrin in acetonitrile (CD_3CN) from T0-T60 mins.....21

14. ^{31}PNMR data spectra analysis of tris(ortho-methoxyphenyl) phosphine with Al-TCPP in acetonitrile (CD_3CN) from T0-T90mins……...……22

15. ^{31}PNMR data spectra analysis of tris(ortho-methoxyphenyl) phosphine with PCN-222 in acetonitrile (CD_3CN) from T0-T90mins…….……..23

16. ^{31}PNMR data spectra analysis of triphenylphosphine with porphyrin in acetonitrile (CD_3CN) from T0-T90mins……..25

17. ^{31}PNMR data spectra analysis of triphenylphosphine with PCN-222 in acetonitrile (CD_3CN) from T0-T60mins…….26

18. ^{31}PNMR data spectra analysis of Triphenylphosphine with PCN-222 in acetonitrile (CD_3CN) T60min with 0.015 as the phosphinate insertion product and 0.9855 as the phosphine oxide product…….26

19. ^{1}HNMR data spectra analysis of 9,10 Dimethyl anthracene with PCN-222 in acetonitrile (CD_3CN) from T0-15min……..29

20. Graph of ln([TPP°]/[TPP*]) vs time (min)……...….31

21. Graph of ln([DMA°]/[DMA*]) vs time(min)……31

CHAPTER 1

Singlet Oxygen: Generation, Reactivity, and Interactions with Aryl Phosphines

Singlet oxygen ($^1O_2$) as the reactive intermediate in photooxidation reaction was first proposed by Kautsky in 1924. However, Kautsky's pioneering work was ignored until seminal studies by Foote and coworkers in 1964.[1,2] Since then, significant breakthroughs and advancements have been made in understanding the photosensitized production of singlet oxygen. Singlet molecular oxygen ($^1O_2$) is a highly reactive form of molecular oxygen distinct from its ground state, triplet oxygen ($^3O_2$). Singlet oxygen studies have covered areas ranging from photooxidation, DNA damage, wastewater treatment, and photodynamic therapy (PDT) of cancer to polymer science.[1]

While singlet oxygen($^1O_2$) and triplet oxygen ($^3O_2$) are two forms of molecular oxygen, singlet oxygen is more reactive due to its electronic configuration and reactivity. The ground state of molecular oxygen ($^3\Sigma_g^-$), also called triplet oxygen ($^3O_2$), has two unpaired electrons with antiparallel spins in the antibonding π^*orbital (Figure 1), the degenerate highest occupied molecular orbital (HOMO).[1] Conversely, the singlet lowest excited state of dioxygen ($^1\Delta_g$), also known as singlet oxygen($^1O_2$), has two paired electrons with parallel spins, leaving an unoccupied antibonding π^*orbital, violating Hund's rule.[1,2] Molecular oxygen can also be excited to a second excited state of singlet oxygen ($^1\Sigma_g^+$), where the spin of an electron can flip and occupy the empty degenerate orbital but is known to be short-lived.[1] The energy difference between the ground state oxygen ($^3\Sigma_g^-$) and its first excited state ($^1\Delta_g$) is 22.5 kcal/mol, while the energy difference between this short-lived excited state ($^1\Sigma_g^+$) and the ground state is 37.5 kcal/mol.[1]

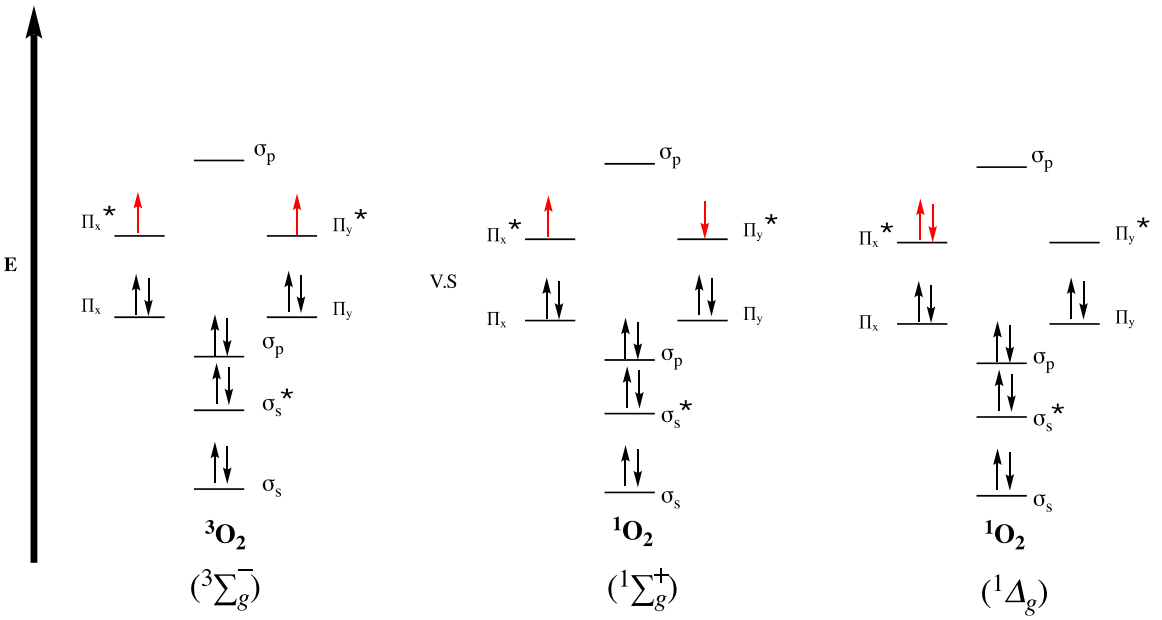


Figure 1: Modified Molecular Orbital Diagram of $^1O_2$ and $^3O_2$.

The spin-forbidden transition from singlet state to triplet ground state leads to a relatively long lifetime of singlet oxygen. The lifetime of singlet oxygen has been measured to be 5 µsec microseconds in water, with a considerably longer lifetime in deuterated solvents.[3] Deuterium, a heavier isotope of hydrogen, significantly impacts the quenching of singlet oxygen by energy transfer. Due to its increased mass, deuterium-containing solvents require more energy to undergo vibrational excitations. This reduced vibrational frequency decreases the energy transfer rate from the singlet oxygen to the solvent molecules, resulting in a prolonged lifetime of the singlet oxygen species. Singlet oxygen is more reactive than triplet oxygen due to the pairing of the electrons in one of the degenerate π* orbitals. This leaves an empty low-lying π* orbital, which nucleophiles can readily attack.

Photosensitization is widely used among the numerous ways to generate singlet oxygen due to its convenient, controllable, and efficient approach. This method includes

a light source, oxygen, and a photosensitizer.[1,2] The singlet oxygen generation pathway (Figure 2) starts with an energy source exciting a ground state photosensitizer P(S_0) to its singlet state P(S_1), which then undergoes intersystem crossing (ISC).[1,2] During the intersystem crossing, the photosensitizer's excited electron intersystem crosses to generate the sensitizer's triplet state P(T_3). Two photooxidation processes from the triplet state may occur Type 1 and Type 2.[1,2,4.] Type 1 involves electron transfer processes and produces radicals or radical ions, while Type 2 produces reactive singlet oxygen through energy transfer between the sensitizer's triplet state and triplet oxygen ($^3O_2$).[4] In the Type 2 mechanism, singlet oxygen reacts with a substrate to produce oxidized and/or oxygenated products.

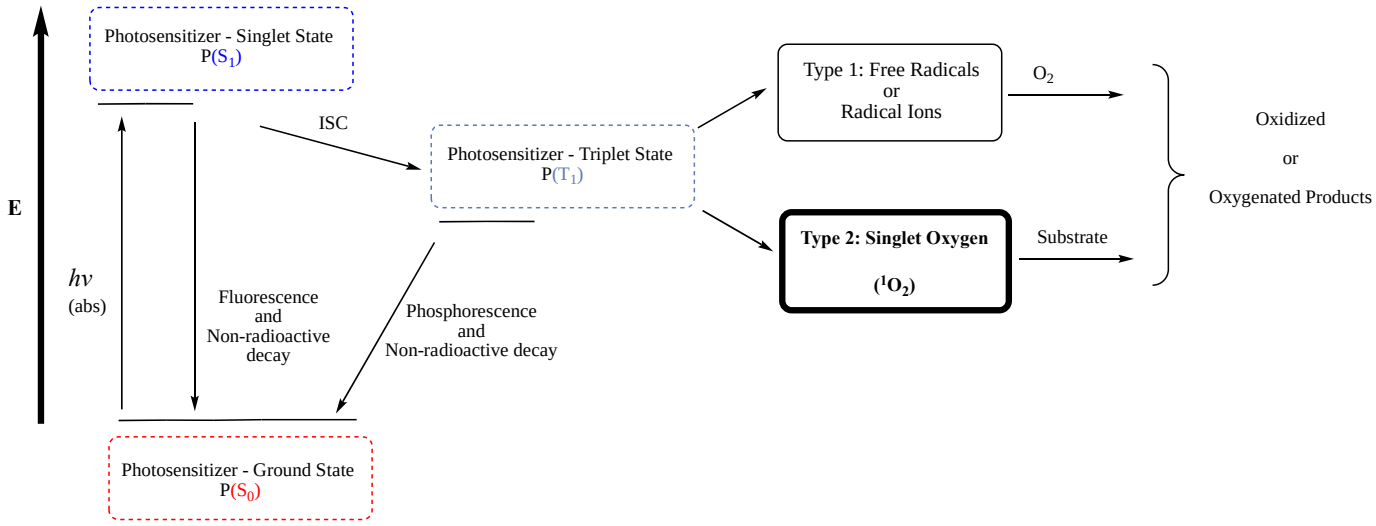


Figure 2. Singlet oxygen pathway via photosensitization with Type 1 and Type 2 mechanisms and products.[1,4]

As mentioned earlier, due to its low-lying LUMO, singlet oxygen is a powerful electrophile. Consequently, it can undergo reactions with π bonds of olefins and dienes as

well as lone pairs of heteroatoms. This includes the singlet oxygen ene reaction, [2+2] cycloaddition, and [4+2] cycloaddition with dienes. Singlet oxygen also reacts with organic sulfides and aryl phosphines. These reactions are depicted in Figure 3 below.

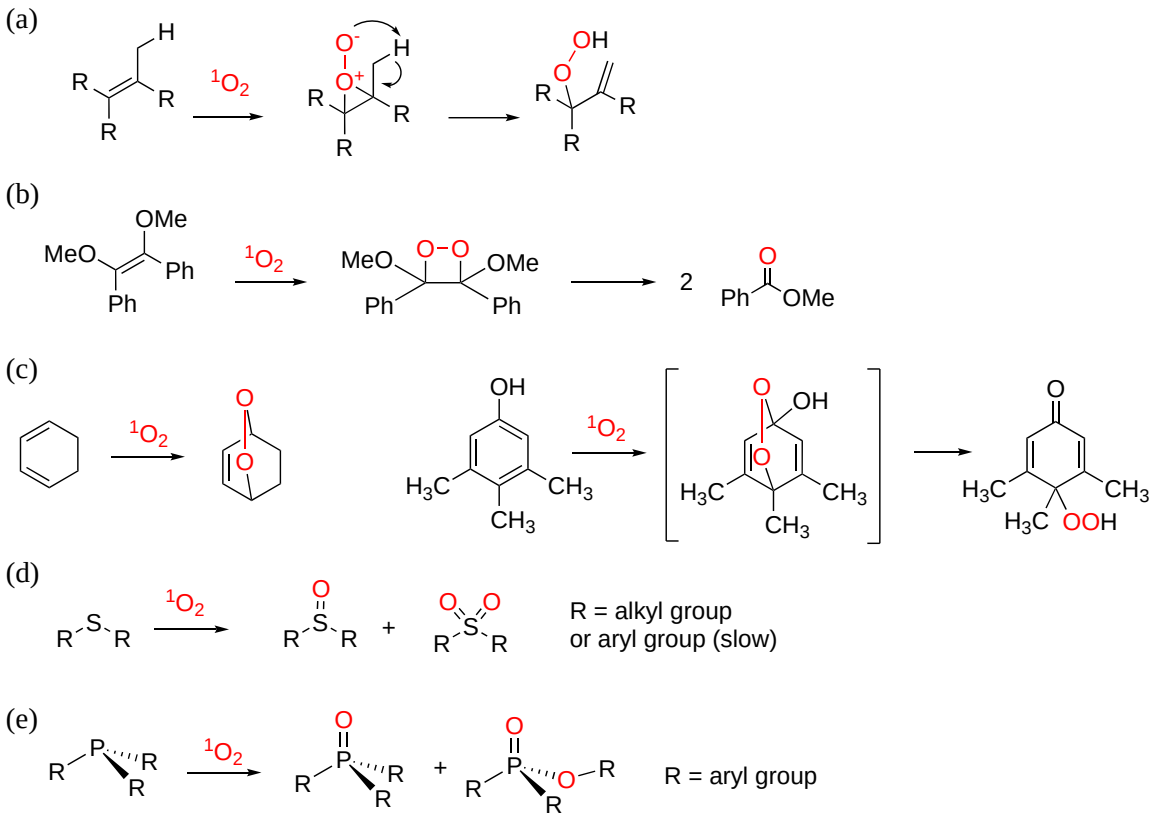


Figure 3. Representative scheme of electrophilic oxidative addition reactions of nucleophiles with singlet oxygen: (a) singlet oxygen ene reaction; (b) [2+2 cycloaddition; (c) [4+2] cycloaddition; (d) photooxidation of sulfides; (e) photooxidation of aryl phosphines.

Trapping of singlet oxygen: 9,10-dimethylanthracene (9,10-DMA) is a polycyclic aromatic hydrocarbon (PAHs) derived from anthracene with the addition of two methyl

groups at the 9 and 10 positions (Figure 4). The reactivity of 9,10-dimethylanthracene (9,10-DMA) and singlet oxygen is well-established: The molecule undergoes [4+2] cycloaddition at the middle ring, making it a selective chemical trap for singlet oxygen. The [4+2] cycloaddition product is a stable endoperoxide, which can be easily detected and quantified, making it a reliable method for studying the generation of singlet oxygen in various systems (Figure 4).[5] Selke and coworkers have determined the rate constant of DMA with singlet oxygen to be $2.5\pm0.1 \times 10^7$ M^{-1} s^{-1} in $CDCl_3$.[6] In CH3CN, the rate has been measured to eb $6.3\pm0.1 \times 10^7$ M^{-1} s^{-1}.[7] With this discovery, studying the comparison of rate constants between 9,10-DMA and other compounds can provide insights into different reaction pathways.

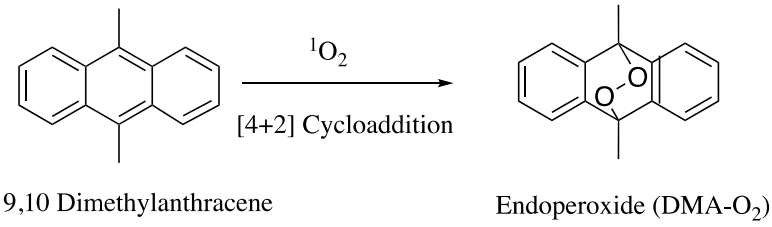


Figure 4: Scheme of singlet oxygen reaction with 9,10 dimethyl anthracene.[5]

Although photooxidation reactions involving alkenes, dienes, and organic sulfides have been well-documented[2,8] the photooxidation of arylphosphines with singlet oxygen remained relatively unexplored until work initiated by the Selke group in the early 2000s. Beyond their use in catalysis and organometallic chemistry, arylphosphines have been explored as fuel stabilizers for jet fuels, and their phosphadioxirane intermediate provided some insights into their antioxidant properties.[6,9]

Arylphosphines are known for their bulky nature. The steric properties of arylphosphines are measured by their cone angle, which plays a massive role in determining their reactivity and coordination behavior.[6,10,11] The cone angle is derived

from a space-filling model of the MP(R3) group (Figure 4) where M is the metal, P is the phosphorus atom of the phosphine ligand, and R are the different substituents on the phosphorus atom.[6] Previous studies investigated the electronic effects of para-substituted arylphosphines and the steric effects of the ortho-substituted arylphosphines.[6,10-13] The chemical reactivity of arylphosphines can be differentiated by their steric bulk, which is indicated by their cone angle. For instance, *para* and *ortho*-substituted aryl phosphines have varying cone angles of 145° and 215°, respectively, yielding different products upon reaction with singlet oxygen.[6,10] The inertness of these arylphosphines towards triplet oxygen paved the way to study their reactivity with singlet oxygen.

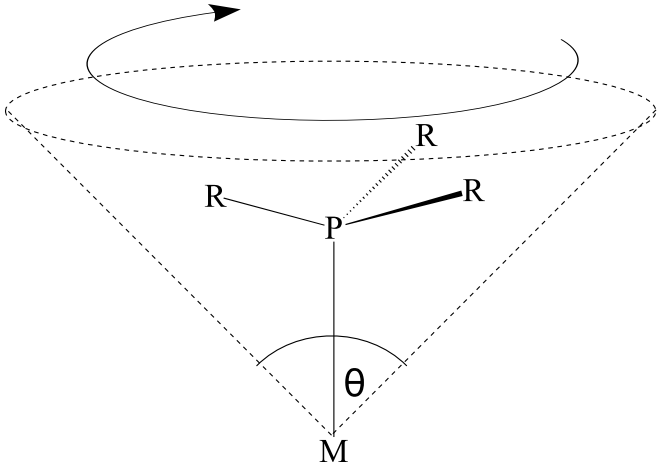


Figure 5: Space-filling model of Tolman's cone angle.[14]

Arylphosphines react with singlet oxygen to form a highly unstable electrophilic intermediate, a phosphadioxirane. This intermediate undergoes an electrophilic oxygen atom transfer with another arylphosphine molecule, or if the approach of the second arylphosphine molecule is severely hindered, the phosphadioxirane intermediate undergoes an intramolecular rearrangement leading to a phosphinate ester (Figure 6).[6,10]

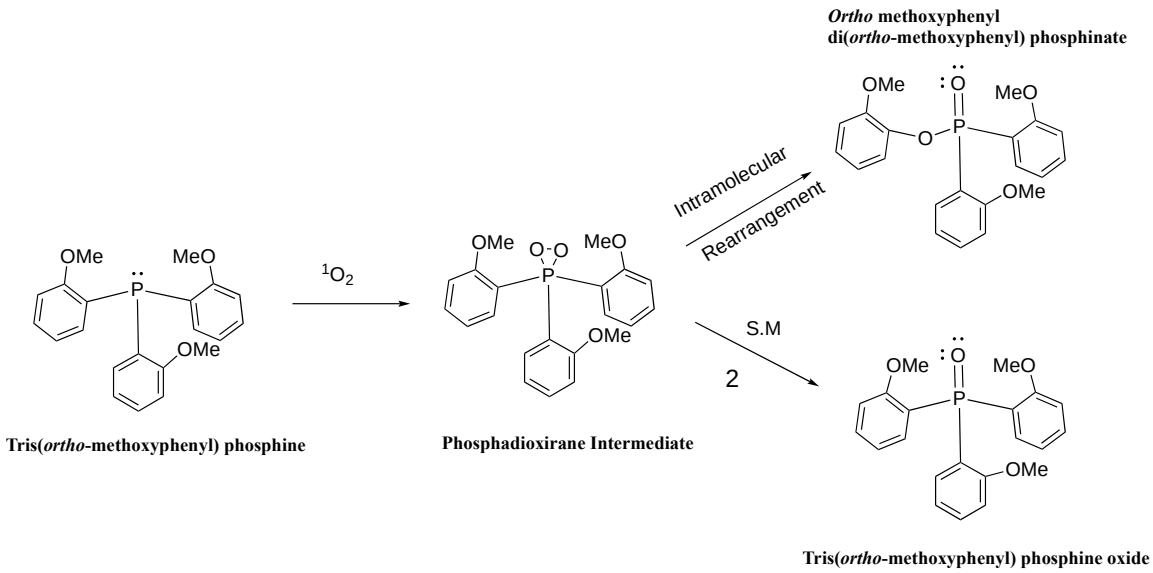


Figure 6: Reaction of singlet oxygen with *ortho*-substituted arylphosphines in a homogeneous media proceeding different pathways yielding two varying products.[6]

To mechanistically understand this process (Figure 7), tris (ortho-methoxyphenyl) phosphine **1** reacts with singlet oxygen. Then, this breaks the π-bond from the singlet oxygen molecule to form a new P-O-O bond, creating a highly strained three-membered ring known as the phosphadioxirane intermediate **I1**. This reactive intermediate is susceptible to ring-opening reactions. The phosphorus and oxygen atoms are electronegatively different, so polarization between the P-O bonds occurs. This causes the phosphorus atom to have a partial positive charge and the oxygen atom to have a partial negative charge. The partially charged phosphorus atom pulls the electrons away from the oxygen atom, which makes the oxygen atom more electron deficient and thus more electrophilic.[6] Due to this, the oxygen atom is prone to react with nucleophiles like another molecule of the starting material or rearrangements of the molecule. There are two different reaction pathways that this intermediate can undergo: the intramolecular pathway and the intermolecular pathway.[6,10] In the intramolecular rearrangement pathway, the alkyl migrates to the less hindered side, forming a new P-O bond and P=O

bond known as the phosphinate ester product **2**. In the intermolecular pathway, a starting material attacks the phosphadioxirane intermediate, forming two phosphine oxide products **3**.[6,10]

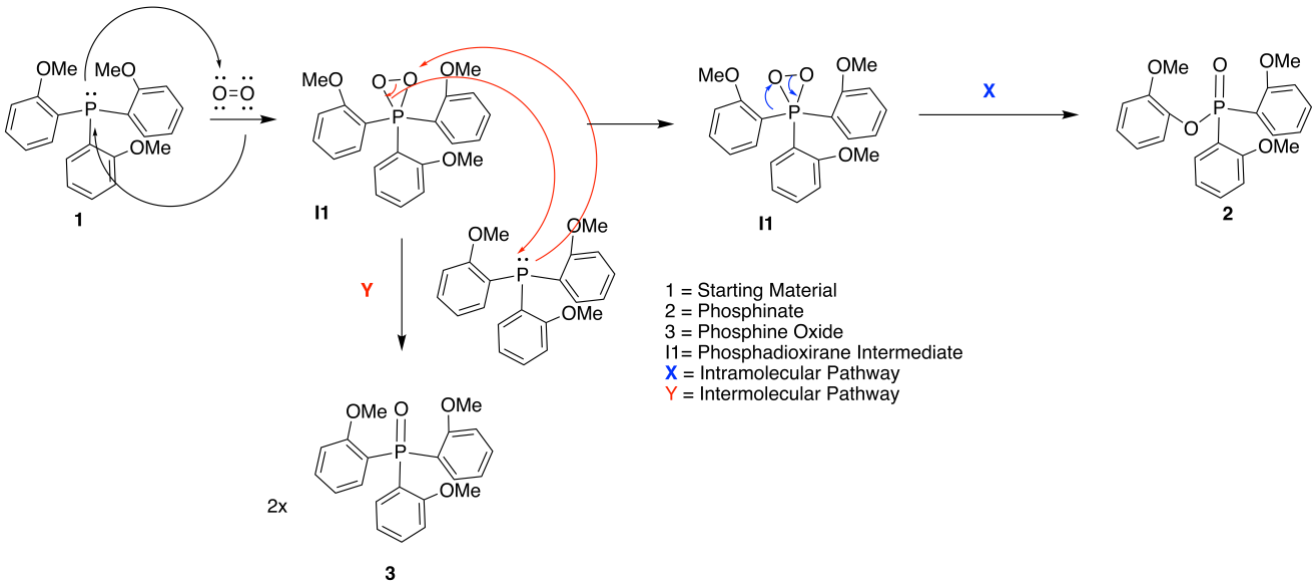


Figure 7: Detailed mechanism of singlet oxygen reaction with tris (ortho-methoxyphenyl) phosphine.

Studies have demonstrated the intramolecular oxygen atom insertion reaction to occur, the substituent in the ortho position is required as the increased steric bulk disfavors a bimolecular intermolecular process.[6,11-13] Selke and coworkers found that the product distribution of the reaction was dependent on the concentration of the starting material: at high concentrations, the intermolecular pathway is favored leading to the formation of two molecules of the phosphine oxide, while at low concentrations, the intramolecular pathway is favored forming the phosphinate ester.[6] This research used triphenylphosphine and tris(ortho-methoxyphenyl) phosphine to study the phosphine oxidation chemistry inside metal-organic frameworks (MOFs). The intermolecular

oxygen atom transfer pathway has much greater steric requirements than the unimolecular reaction pathway. Therefore, if the reaction of aryl phosphines occurs inside the MOF pores, the unimolecular rearrangement to form phosphinate esters should be favored compared to reactivity in a homogeneous solution. On the other hand, if the reaction does not occur inside the MOF pores, the product distribution should be similar to that found in homogeneous solutions. We, therefore, hypothesize that aryl phosphines can be used as mechanical probes to investigate if singlet oxygen reactions catalyzed by MOFs take place inside or outside the crystalline framework of the material.

CHAPTER 2

Porphyrin-Based Metal-Organic Frameworks

Porphyrins are fundamentally crucial as ligands and dyes in biological and natural systems. They form the core structure of vital compounds such as heme in hemoglobin (iron-porphyrin complex), hemocyanin (copper-porphyrin complex) in many animals, chlorophyll (magnesium-porphyrin complex) in plants, and vitamin B12 (cobalt-porphyrin complex).[14] Aside from the critical roles in various biological processes, including oxygen transport, photosynthesis, and cellular respiration, porphyrin moieties within a metal-organic framework act as a photosensitizer to generate singlet oxygen.[14,15]

Metal-organic frameworks (MOFs) are porous crystalline structures composed of inorganic metal nodes/clusters and organic linkers/ligands, which contribute to their tunable nature as catalysts (Figure 8).[16] MOFs are composed of metal ions or metal clusters that are connected by organic linkers. The metal centers can range from single metal ions to larger clusters, while the organic linkers are carbon-based molecules that act as bridges between these metal units.[16] The metal ions and organic linkers are held together by coordinate covalent bonds, forming a porous framework structure.[16] MOFs, renowned for their capacity to confine and store molecules, have found applications in diverse fields such as gas storage and separation, catalysis, drug delivery, and energy storage.[16]

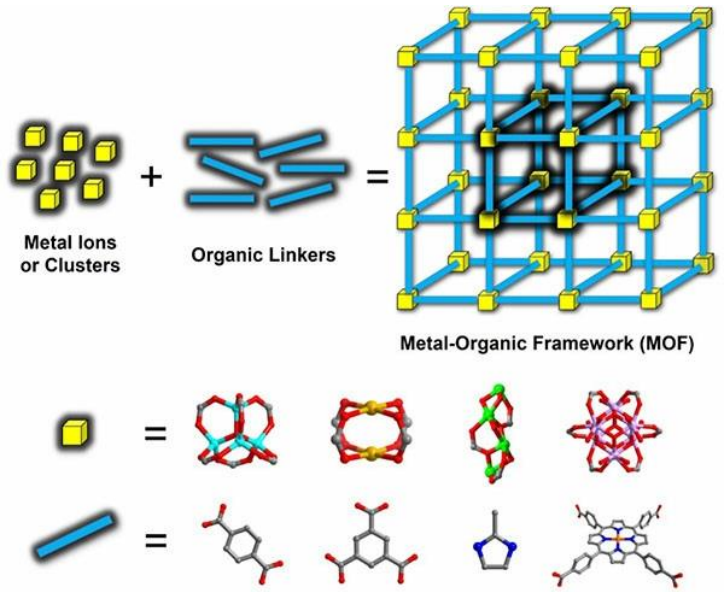


Figure 8: A three-dimensional model of a MOF structure

Al-TCPP and PCN-222 are two distinct MOFs that incorporate porphyrin linkers and have been studied as catalysts for singlet oxygen generation. Al-TCPP has an aluminum metal center and was reported to be one of the most chemically and thermally stable MOF with a BET surface area of 1,400 m^2g^{-1}.[17] PCN-222, a MOF with a zirconium metal center, is similarly known for its stability, but has a higher reported BET surface area of 2,223m^2g^{-1}.[18] Zirconium-based MOFs have gained significant attention due to their chemical stability in various solvents and harsh conditions preventing degradation.[19] Their thermal stability also allows them to withstand elevated temperatures without structural degradation.[19] Recent studies have determined the singlet oxygen quantum yield of PCN-222 MOF to be 0.35 ± 0.02.[20] With their multifunctionality properties, MOFs (with a specific pore environment) also exhibit confinement effects where the different active sites can influence the reactivity between the substrate and catalyst inside the cage (Figure 9).[21] This research investigated the caging effects of MOFs, their

reactivity with aryl phosphines, and whether singlet oxygen diffuses in or out of the MOF cage.

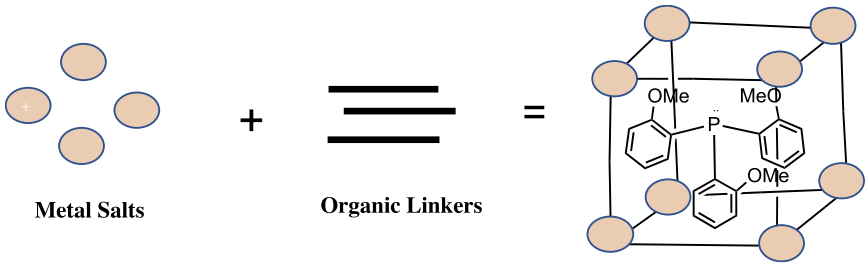


Figure 9: Model Scheme of a MOF cage confining tris(ortho methoxyphenyl) phosphine

CHAPTER 3

Metal-Organic Frameworks (MOFs): Synthesis and Characterization

3.1 Materials

Meso-tetra(4-carboxyphenyl) porphyrin (TCPP, 97%), *N, N*-dimethylformamide (DMF, 99.9%), aluminum trichloride hexahydrate ($AlCl_3 \cdot 6H_2O$, 99.9%), were purchased from Frontier Scientific. Zirconium chloride ($ZrCl_4$ >99.5%) was obtained from Alfa Aesar. Acetone was purchased from Sigma-Aldrich. D_3-acetonitirle (CD_3CN, 99.5%) was obtained from Cambridge Isotope Laboratories.

3.2 Instrumentation

Powder X-ray Diffraction (PXRD) was utilized for phase identifications and purity analysis of the MOF. The Powder X-ray Diffraction (PXRD) spectrums were collected on a D2 Phaser equipped with a Cu-sealed tube ($\lambda = 1.54178$) at 30 kV and 10 mA, over a range of 2-20° with a step size of $2\theta = 0.01°$ (1 second per step). The nitrogen isotherm (N_2 isotherm) was used for N_2 adsorption measurements, which provides Brunauer-Emmett-Teller (BET) surface areas, and pore distribution of all MOFs were determined on a Micromeritics ASAP 2020 Plus. ^{1}H NMR and ^{31}P NMR spectra were obtained using a Bruker 400 MHz NMR spectrometer. The MOF and phosphine solution were irradiated by a 250 W tungsten halogen lamp (set at 12 A) with a cutoff filter at 493nm.

3.3 Synthesis of Al-TCPP

The synthesis of Al-TCPP followed the procedure outlined by Fateeva's group. A mixture of 0.126 mmol of 5,10,15,20-tetrakis(4-carboxyphenyl) porphyrin (TCPP) and 0.25 mmol of aluminum chloride hexahydrate ($AlCl_3 \cdot 6H_2O$) was dissolved in 10 mL of deionized water. The resulting suspension was sonicated for 20 minutes to ensure homogeneity. The

reaction mixture was then transferred to a Teflon-lined autoclave reactor and heated to 160 °C for 16 hours in a programmable oven. Subsequently, the autoclave was cooled gradually at a rate of 1.5 °C/minute to room temperature. The solid product was isolated by centrifugation and washed thoroughly with dimethylformamide (DMF) (3 x 15mL) and acetone (3 x 15mL) to remove any unreacted starting materials or byproducts. The washed product was then dried in a vacuum oven at room temperature before activation, yielding a burgundy-red powder.

3.4 Synthesis of PCN-222

The synthesis of PCN-222 was adapted from Hao and coworkers. A mixture was prepared by dissolving 14 mg (0.06 mmol) of zirconium chloride ($ZrCl_4$), 20 mg (0.025 mmol) of porphyrin (H_2TCPP), and 5.64 mL of formic acid in 20 mL of dimethylformamide (DMF). The solution was transferred to an ultrasonic bath (CPX2800 Fischerbrand) for about 10-20 minutes to ensure the components in the solution reached complete dissolution. The solution was placed in the oven (Shel lab) and heated at 120 °C for 18 hours. Then, the solution was cooled to room temperature, where dark purple crystals formed through precipitation. The sample was washed with DMF (3 x 20 mL with the third time left overnight) and acetone (3 x 20 mL with the third time left overnight). After, the sample was dried in a vacuum at room temperature for at least 2 hours before activation.

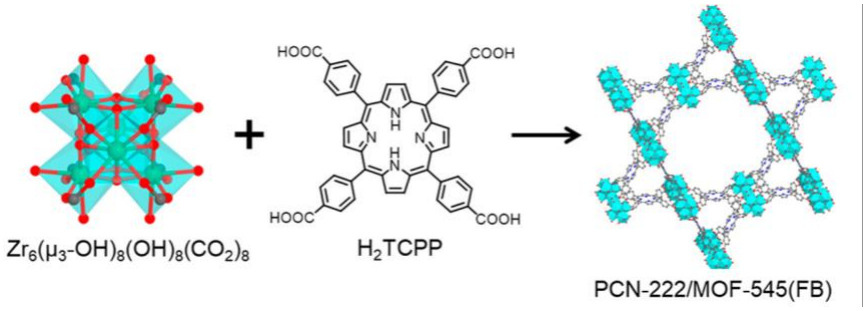


Figure 10: A reaction scheme for synthesizing PCN-222 with zirconium as the metal salt and TCPP as the organic linker.

3.5 Characterization of MOFs

To analyze the physical orientation of MOFs, powder x-ray diffraction pattern (PXRD) was utilized to measure the crystal structure, phase purity, and lattice dimensions. Nitrogen adsorption/ desorption isotherm (N_2 Isotherm) was also used to determine the surface area, pore size distribution of the MOF, and the adsorption/ desorption behavior. The PXRD results of Al-TCPP (Figure 11) and PCN-222 (Figure 12) confirmed the crystal structure and lattice dimensions since the experimental matched the simulation literature value. After validating the lattice crystalline structure, the MOFs were prepared for further analysis by activating N_2 adsorption and isotherm. This process removes any residual solvent from the MOFs by heating them to a high temperature and then filling the pores with N_2 gas. Once fully activated, the MOFs were characterized using BET theory and density functional theory (DFT) to determine their surface area and pore diameter from the isotherm data.[23] The level of theory was determined by 2020 ASAP (Accelerated Surface Area and Porosimeter System). The synthesized MOFs exhibited the desired pore diameter and surface area (Table 1) and were stored in the desiccator.

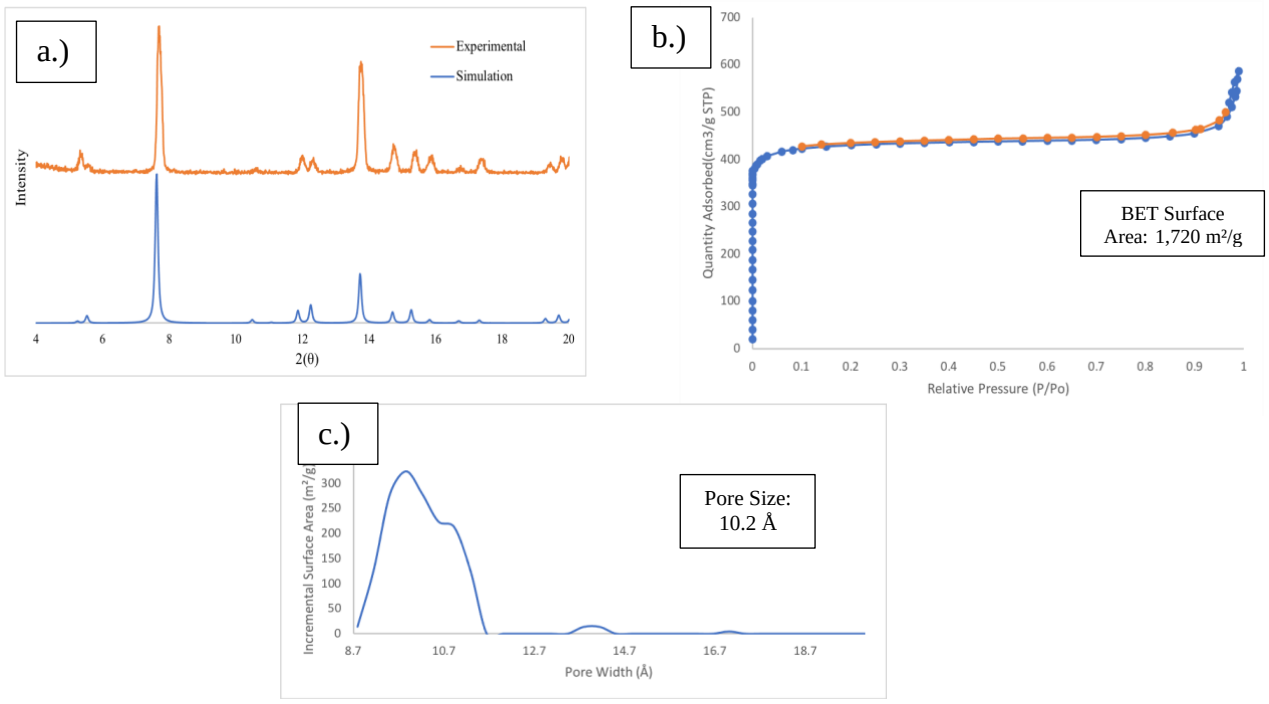


Figure 11: Al-TCPP MOF (a)Powder X-ray Diffraction (PXRD), (b)Nitrogen Adsorption/ Desorption Isotherm (N_2 Isotherm) Analysis, and (c)DFT Pore Size Distribution

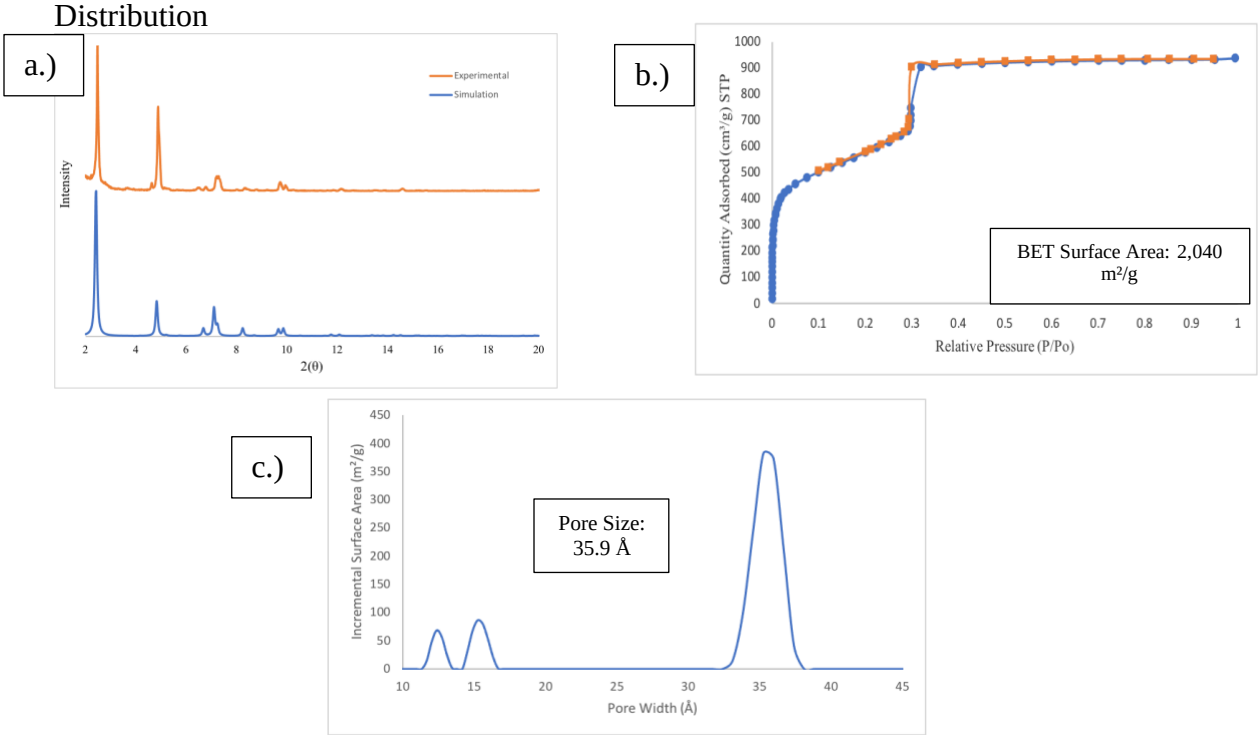


Figure 12: PCN-222 MOF (a)Powder X-ray Diffraction Pattern (PXRD), (b)Nitrogen Adsorption/ Desorption Isotherm (N_2 Isotherm) Analysis, (c) DFT Pore Size Distribution

CHAPTER 4

Photooxidation of Arylphosphines and 9,10 Dimethyl anthracene in Porphyrin and MOFs: Results

4.1 Materials

Tris(ortho-methoxyphenyl) phosphine (98%) was purchased from Strem Chemicals. Triphenylphosphine (99%) was obtained from Aldrich. Meso-tetra(4-carboxyphenyl) porphyrin (TCPP, 97%) was acquired from Frontier Scientific. Acetone was purchased from Sigma-Aldrich. D3-acetonitirle (CD3CN, 99.5%) was obtained from Cambridge Isotope Laboratories. Bruker Avance II 400 MHz NMR (Nuclear Magnetic Resonance) with Topspin NMR software ^{31}PNMR (1,024 scans) and ^{1}HNMR (256 scans) was utilized.

4.2 Photooxidation Reactions with MOFs

4.2.1. General Procedure for the Photooxidation of Arylphosphines in Porphyrin and Porphyrin-based MOFs

Photooxidation experiments were conducted with a deuterated aprotic solvent, acetonitrile-d3, with a consistently slow steam of O_2 bubbling through the solution. Note that protic solvents cannot be used for this study, as phosphadioxirane has been shown to readily be protonated in such solvents, leading to the formation of hydroperoxides. The photooxidation of the arylphosphines in porphyrin and MOFs utilized a 250 W tungsten halogen lamp (set at 12 A) with a cutoff filter at 493 nm. The phosphine, MOF/porphyrin, and solvent mixture were placed in a glass test tube. A 5% catalyst loading of the MOF was utilized. We measured a concentration of arylphosphines (26.2 mg of triphenylphosphine and 35.2mg of tris (ortho-methoxyphenyl) phosphine) in 2 mL of

acetonitrile-d3. Then, the solution was subjected to sonification for 20 minutes to improve the dissolution of the solute. After sonification, a consistent slow steam of O_2 was bubbled at one bubble per second through the solution. At the same time, it was irradiated using the 250 W tungsten halogen lamp (set at 12 A) with a cutoff filter at 493 nm. Samples were collected at various irradiation times: 0 min, 5 mins, 10 mins, 15 mins, 30 mins, 60 mins, and 90 mins. ^{31}PNMR was used to analyze product formation and yields.

4.2.2. General Procedure for the Photooxidation of 9,10-Dimethylanthracene in Porphyrin and Porphyrin based MOFs

Photooxidation experiments were conducted with the deuterated aprotic solvent acetonitrile-d3, with a consistently slow steam of O_2 bubbling through the solution, as described in the previous section. We used a 50mMolar of 9,10-dimethylanthracene (20.6mgs) in 2ml of acetonitrile-d3. Product yields were quantified by integrating the aromatic protons of the starting material at 8.34 ppm (4 H) and 7.55 ppm (4 H) and those of the product endoperoxide at 7.46 ppm (4 H) and 7.32 ppm (4 H).

4.3 Results

4.3.1 Photooxidation of Tris(ortho-methoxyphenyl) phosphine in Al-TCPP Meso-tetra(4-carboxyphenyl) porphyrin

The pore size of Al-TCPP is 10.2 Å. This is just slightly larger than the size of one phosphine molecule. Therefore, a bimolecular reaction (formation of phosphine oxide) is impossible inside the MOF pores: For the intermolecular process to occur, two molecules of the starting material must be able to fit in the pore size.

We first studied the reaction of tris(ortho-methoxyphenyl) phosphine in a homogeneous solution (CD_3CN) (35.2 mg, 50 mM) using Meso-tetra(4-carboxyphenyl) porphyrin as a photosensitizer. The time course of this reaction (0 – 60 min) is depicted in Fig. 13. The reaction was followed by ^{31}P NMR with spectra recorded after 15 min irradiation intervals. The product was determined to be tris(ortho-methoxyphenyl) phosphine oxide, as the product peak at 22.2 ppm is in good agreement with the literature value for tris(ortho-methoxyphenyl) phosphine oxide from previous studies.[6]

We then investigated the same reaction using two different MOFs as photocatalysts. To ensure that the quantity of porphyrin is the same with the porphyrin-based MOFs, we calculated the porphyrin unit in each MOF. We multiplied the catalyst loading by the moles used of the substrate and by the molecular weight of MOF and then divided that by the porphyrin unit of the MOF to determine how much of the MOF in mg was needed i.e. $x(mg) of\ MOF = \frac{catalyst\ loading \times mmoles\ used\ of\ substrate \times molecular\ weight\ of\ MOF}{porphyrin\ unit\ in\ MOF}$.

First, we employed Al-TCPP. We use 35.2 mg of tris(ortho-methoxyphenyl) phosphine (50 mM) and 2.20 mg of Al-TCPP. The reaction was again followed by ^{31}P NMR. The time course of this reaction is shown in Fig. 14. Again, the left peak at 22.2 ppm

(phosphine oxide product) grows over time while the right peak at -38.7 ppm (starting material, i.e., tris(ortho-methoxyphenyl) phosphine) disappears. As can be seen from the spectra in Figures 13 – 14, the reaction process for the Al-TCPP MOF is considerably faster than that of the homogeneous solution with the free porphyrin; in fact, the Al-MOF-catalyzed reaction goes to completion within one hour.

4.3.2 Photooxidation of Tris(ortho-methoxyphenyl) phosphine in PCN-222

We also investigated the MOF PCN-222 as a photocatalyst. PCN-222 has a larger pore size of 35.9Å, about triple the size of Al-TCPP. It should, therefore, be easy for at least one molecule of tris(ortho-methoxyphenyl) phosphine to enter the pores of this MOF. The time course for this reaction is depicted in Figure 15. This reaction was slower than the one catalyzed by the Aluminum MOF, and it did not complete within one hour. The reaction was just slightly faster than that of the free base porphyrin: Figure 13 and Figure 15 at 60 mins show a conversion ratio (product: starting material) of 0.46/0.53 (Table 1) and 0.39/0.61 (Table 3), respectively.

It should be noted that in all cases, the phosphine oxide was the sole product. We conclude that all the photooxidation of tris(ortho-methoxyphenyl) phosphine in Al-TCPP must occur outside the MOF. Since the pore size of this MOF is barely larger than that of the phosphine, it may be difficult for even one phosphine molecule to enter the MOF pore. We, therefore, used MOFs with a larger pore diameter for subsequent experiments.

The above experiment shows that singlet oxygen can readily diffuse out of the MOF and undergo reactions that appear identical to those in a homogeneous solution. The ^{31}P NMR results for this MOF are shown in Figure 14 below.

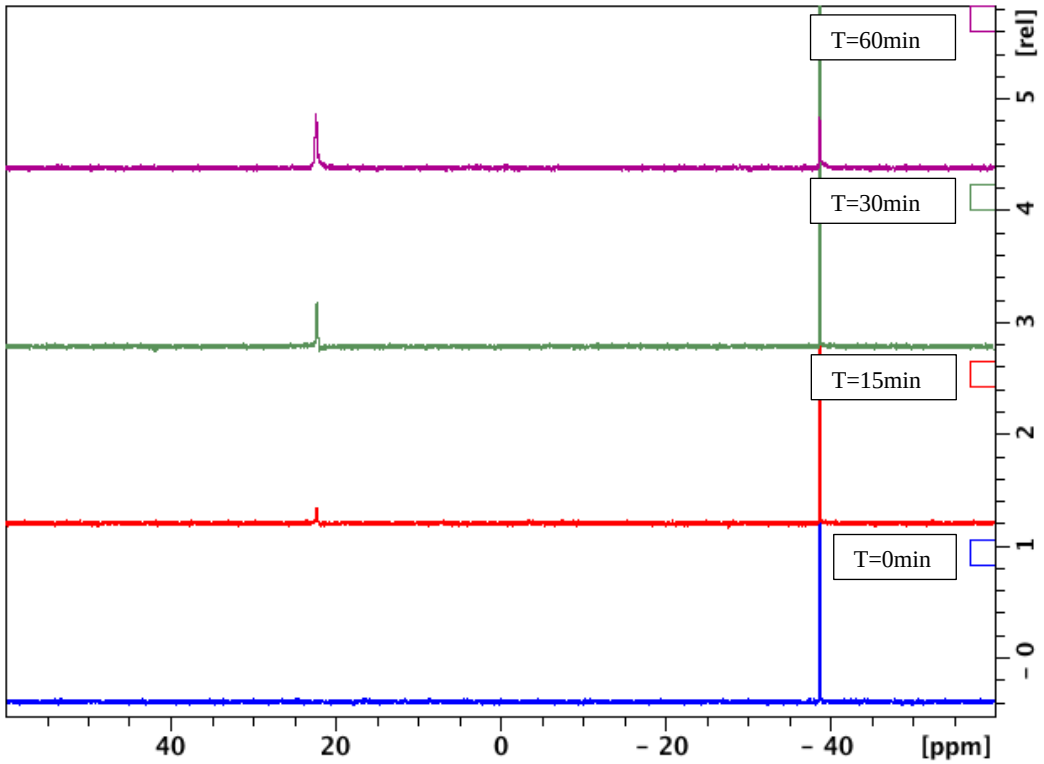


Figure 13: ^{31}PNMR data spectra analysis of tris(ortho-methoxyphenyl) phosphine with Meso-tetra(4-carboxyphenyl) porphyrin in acetonitrile (CD_3CN) from T0-T60 mins.

Time (min)	S.M. Integral values	P Integral values	P:SM ratios
0	1.00	0	0.00/1.00
15	0.92	0.08	0.08/0.92
30	0.83	0.17	0.17/0.83
60	0.53	0.46	0.46/0.53

Table 1: Integration of ^{31}P NMR peaks from Figure 13 of the product and starting material ratios with respect to time in minutes.

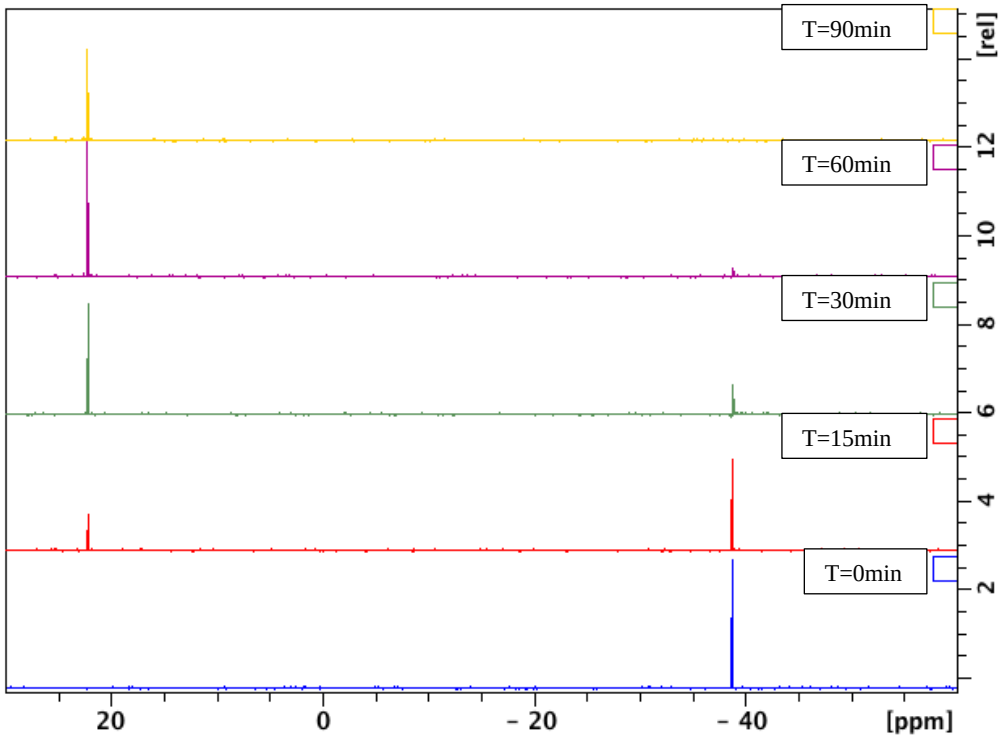


Figure 14: ^{31}PNMR data spectra analysis of tris(ortho-methoxyphenyl) phosphine with Al-TCPP in acetonitrile (CD_3CN) from T0-T90mins.

Time (min)	S.M. Integral values	P Integral values	P:SM ratios
0	1.00	0.00	0.00/1.00
15	0.67	0.33	0.33/0.67
30	0.36	0.64	0.64/0.36
60	0.06	0.94	0.94/0.06
90	0.00	1.00	1.00/0.00

Table 2: Integration of ^{31}P NMR peaks from Figure 14 of the product and starting material ratios with respect to time in minutes.

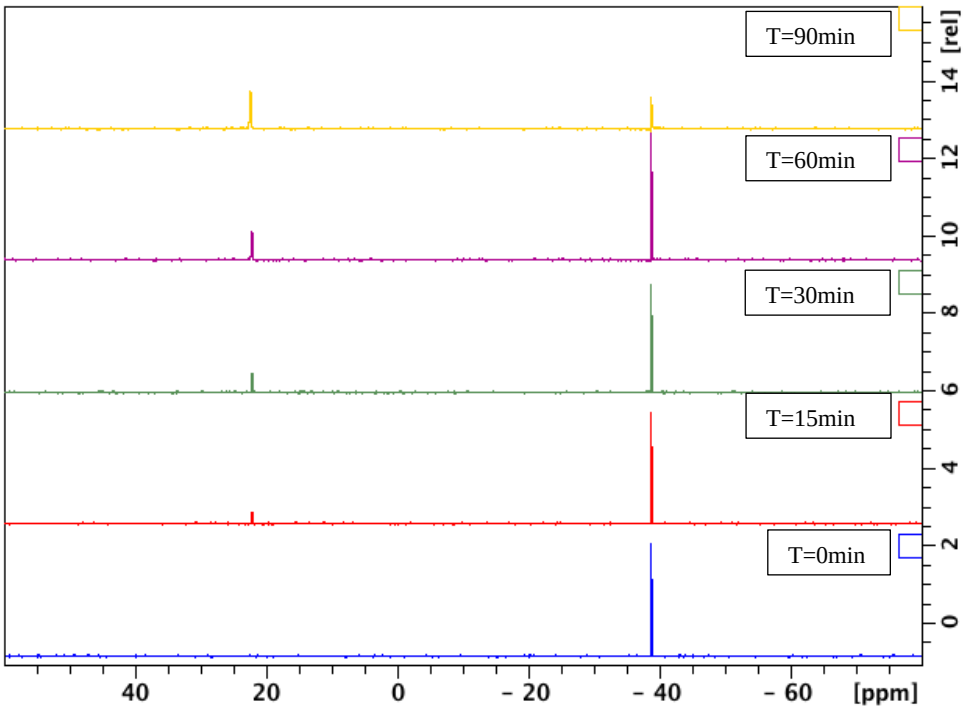


Figure 15: ^{31}PNMR data spectra analysis of tris(ortho-methoxyphenyl) phosphine with PCN-222 in acetonitrile (CD_3CN) from T0-T90mins.

Time (min)	S.M. Integral values	P Integral values	P:SM ratios
0	1.00	0	0.00/1.00
15	0.79	0.21	0.79/0.21
30	0.70	0.30	0.70/0.30
60	0.61	0.39	0.39/0.61
90	0.55	0.44	0.44/0.55

Table 3: Integration of ^{31}P NMR peaks from Figure 15 of the product and starting material ratios with respect to time in minutes.

4.3.3 Photooxidation of Triphenylphosphine (TPP) with Meso-tetra(4-carboxyphenyl) porphyrin and PCN-222

We then investigated the reaction of triphenylphosphine with the free base porphyrin and PCN-222. As seen in Figure 16 and Figure 17, Triphenylphosphine reacts slower in a homogeneous solution with Meso-tetra(4-carboxyphenyl) porphyrin as a sensitizer than the PCN-222 MOF. In Table 4, we also observe that in 60min, there is barely a 51:49 conversion for porphyrin, while in Table 5, we see there's complete conversion by 60 min for PCN-222. The starting material is the right peak at -6.04 ppm, and the phosphine oxide product peak is the left peak at 26.2 ppm. The values of the ^{31}P NMR peaks are in agreement with the literature.[5] Table 1 and Table 2 show the integrated values of the starting material and product. Both reactions yield a phosphine oxide and about 1 % of the phosphinate insertion product formed by intramolecular rearrangement (Figure 18). The insertion product is not enhanced when the PCN-222 MOF is employed.

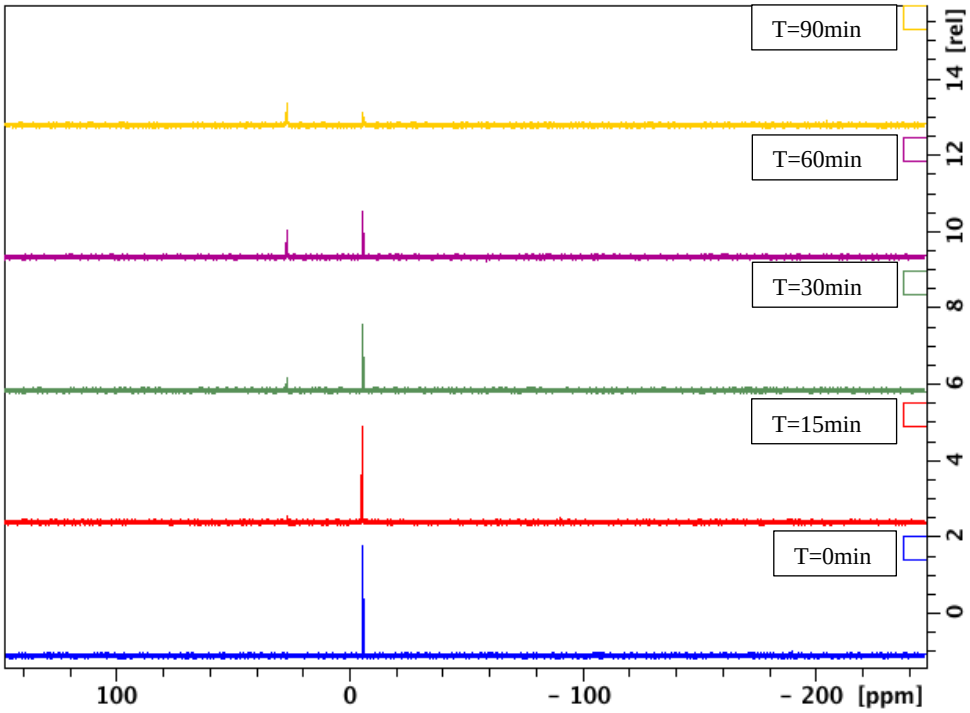


Figure 16: ^{31}PNMR data spectra analysis of triphenylphosphine with porphyrin in acetonitrile (CD_3CN) from T0-T90mins.

Time (min)	S.M. Integral values	P Integral values	P:SM ratios
0	1.00	0	0.00/1.00
15	0.93	0.07	0.07/0.93
30	0.83	0.17	0.17/0.83
60	0.51	0.49	0.49/0.51
90	0.24	0.76	0.76/0.24

Table 4: Integration of ^{31}P NMR peaks Integral values from Figure 16 of the product and starting material ratios with respect to time in minutes.

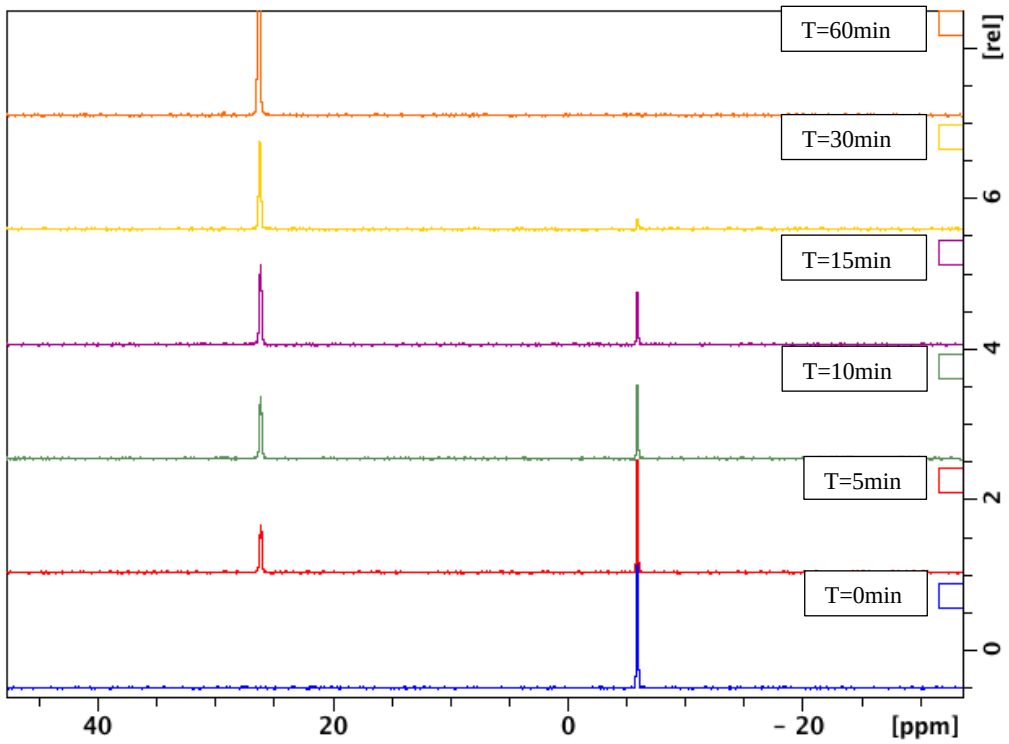


Figure 17: ^{31}PNMR data spectra analysis of triphenylphosphine with PCN-222 in acetonitrile (CD_3CN) from T0-T60mins.

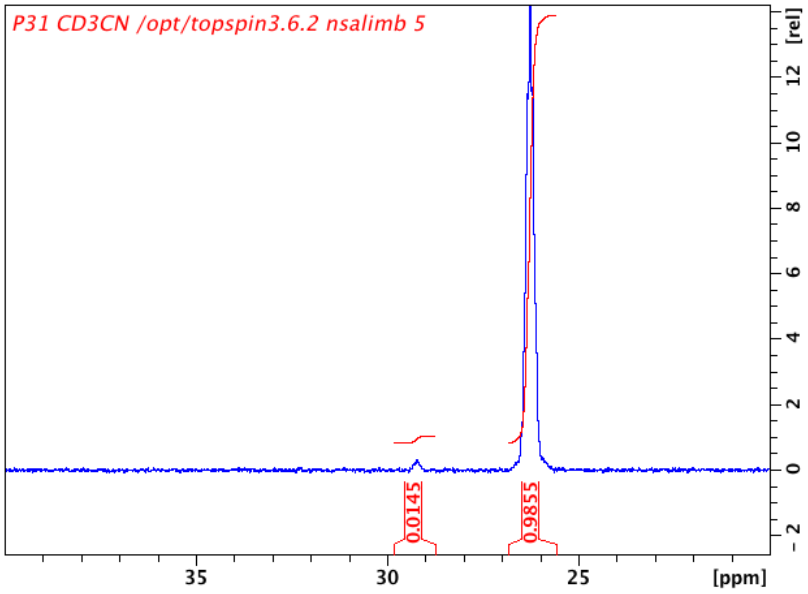


Figure 18: ^{31}PNMR data spectra analysis of Triphenylphosphine with PCN-222 in acetonitrile (CD_3CN) T60min with 0.015 as the phosphinate insertion product and 0.9855 as the phosphine oxide product.

Time (min)	S.M. Integral values	P Integral values	P:SM ratios
0	1.00	0	0.00/1.00
5	0.57	0.43	0.43/0.57
10	0.40	0.60	0.60/0.40
15	0.27	0.73	0.73/0.27
30	0.07	0.93	0.93/0.07
60	0	1.00	1.00/0.00

Table 5: Integration of ^{31}P NMR Peaks from Figure 17 of the product and starting material ratios with respect to time in minutes.

4.4. Comparison of Relative Rate Constants for Photooxidation of Triphenyl Phosphine in PCN-222 and Homogenous Solution with Rate Constants for Photooxidation of 9,10-Dimethylanthracene (DMA) Catalyzed by PCN 222 and in Homogeneous Solution

The chemical reaction rate constant k_r for the reaction of triphenylphosphine with singlet oxygen has been determined to be 1.6 x 10^7 $M^{-1}sec^{-1}$.[6] Likewise, the rate constant for the reaction of DMA with singlet oxygen has been determined to be 6.3 x 10^7 $M^{-1}sec^{-1}$.[7] Hence, DMA reacts four times faster than triphenylphosphine with singlet oxygen in a homogeneous solution. We can use the data from the time course of the reaction of singlet oxygen with triphenylphosphine catalyzed by PCN-222 to obtain the first-order rate of disappearance of the starting phosphine molecule. We then conduct a similar time course study with the reaction of singlet oxygen with DMA to determine if the rate constant ratio changes when MOFs are employed as sensitizers instead of dyes in a homogeneous solution. The reaction of the phosphine or DMA with singlet oxygen is second-order overall (first-order in substrate concentration and first-order in singlet oxygen concentration). However, suppose identical amounts of the MOFs are used for the phosphine and the DMA experiments with similar irradiation conditions. In that case, the

singlet oxygen concentration should be the same for both time courses, allowing a direct comparison of the first-order decay rates for each starting material.

4.4.1 Photooxidation of 9,10 Dimethyl anthracene with PCN-222

We used 20.6 mg (50 mM) of DMA and 3.0 mg of PCN-222 and followed the DMA disappearance by ^{1}H NMR. The photooxidation reaction of DMA in PCN-222 (Figure 19) is considerably faster than that of triphenylphosphine: The starting material is wholly consumed after just 15 minutes. The starting material peaks determined for DMA in the aromatic region are 8.34 ppm (m, 4 H) and 7.55 ppm (m, 4 H), and those of the product endoperoxide at 7.46 ppm (m, 4 H) and 7.32 ppm (m, 4 H). We use these proton signals for the integration in Figure 19 as they are easier to integrate than the methyl-group protons, which are too close to solvent peaks for reliable integration.

Time (min)	Integral values (SM)	Integral values (P)	P:SM ratios
0	1.99	0.00	1.99/0.00
5	0.07	0.24	0.24/0.07
10	0.02	0.33	0.33/0.02
15	0.01	0.34	0.34/0.01

Table 6: Integral values from Figure 19 of the product (DMA-O_2) and starting material (DMA) ratios with respect to time in minutes.

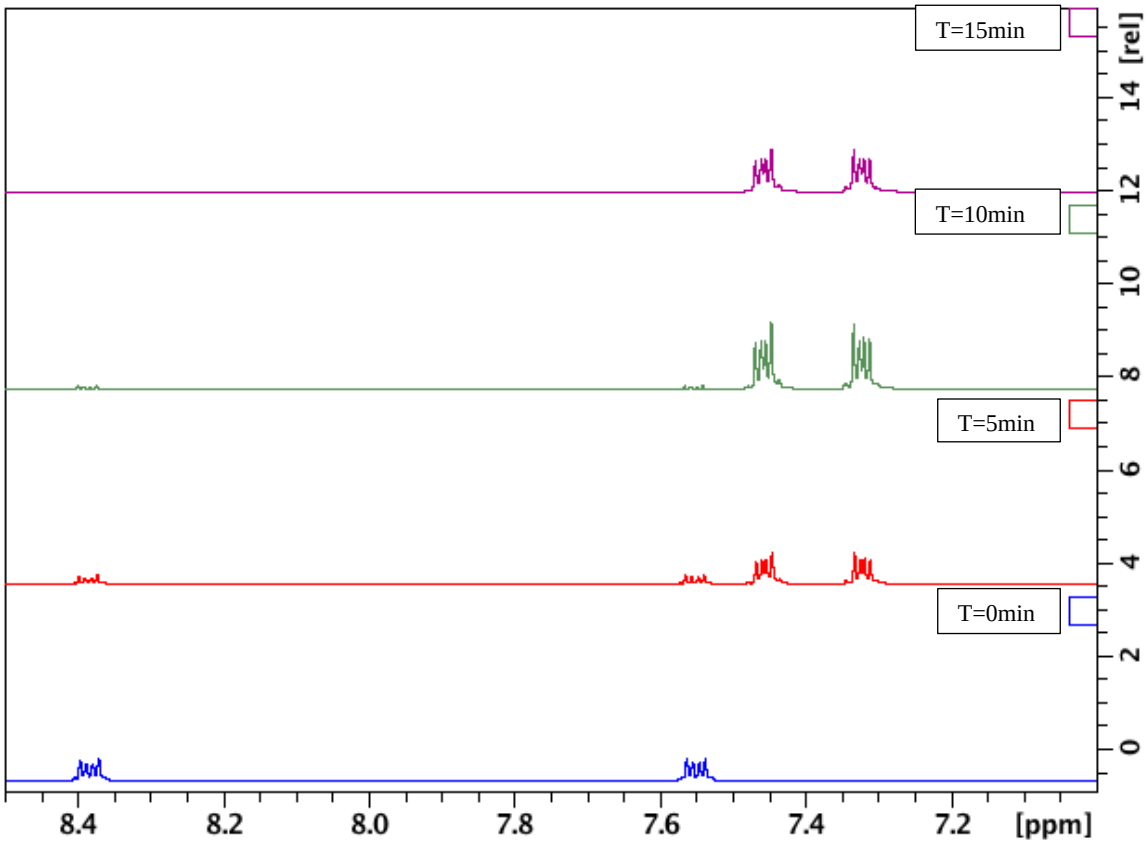


Figure 19: ^{1}HNMR data spectra analysis of 9,10 Dimethyl anthracene with PCN-222 in acetonitrile (CD_3CN) from T0-15min.

4.4.2 Rate of Disappearance Analysis and Comparison of Rate Constants of 9,10 Dimethylanthracene and Triphenylphosphine with PCN-222

To obtain the first-order rate constants for the disappearance of the starting compounds, we plotted $\ln([A°]/[A^x]$ vs time (min) where A represents the substrate, [A°] is the sum of both peak integrals at a given time and $[A^x]$ is the integral of starting material left at time x. Figure 20 and Figure 21 both show a linear relationship between $\ln([A]°/ [A^x])$ and time and a first-order reaction, meaning that the rate of TPP and DMA disappearance is directly proportional to its concentration at any given time. The ratio of the slopes in

Figure 20 and Figure 21 corresponds to the rate constant (*k*r) ratios of the triphenylphosphine and DMA reaction with singlet oxygen catalyzed by PCN-222. The ratios of the slopes = k_{DMA}/k_{TPP} = 3.4. This indicates that the reaction of DMA with singlet oxygen within the PCN-222 MOF is approximately 3.4 times faster than the reaction of TPP under the same conditions. As mentioned in the introduction to this section, the rate constant for DMA photooxidation in acetonitrile solution is reported as $6.3 \pm 0.1 \times 10^7$ $M^{-1}s^{-1}$,[7] while that of triphenylphosphine is 1.6×10^7 $M^{-1}sec^{-1}$ in homogeneous solution. The rate constant ratio of 3.4 for the two MOF-catalyzed reactions is very close to the rate constant ratio of 4.0 in a homogeneous solution. We know from the lack of insertion product formation that the triphenylphosphine reacts outside the MOF pores with singlet oxygen. Since the rate constant ratio between the photooxidation of DMA and phosphine does not change from homogenous solution to the PCN-222-catalyzed reactions, DMA likely reacts primarily with singlet oxygen molecules that have diffused from the MOF pores. Using this methodology for other smaller substrates will be interesting and more likely to diffuse into the MOF pores. If the reaction rate ratio for such substrates vs. triphenyl phosphine increased compared to the rate constant ratio in inhomogeneous solutions, there would be evidence for reaction inside and outside the MOF pores.

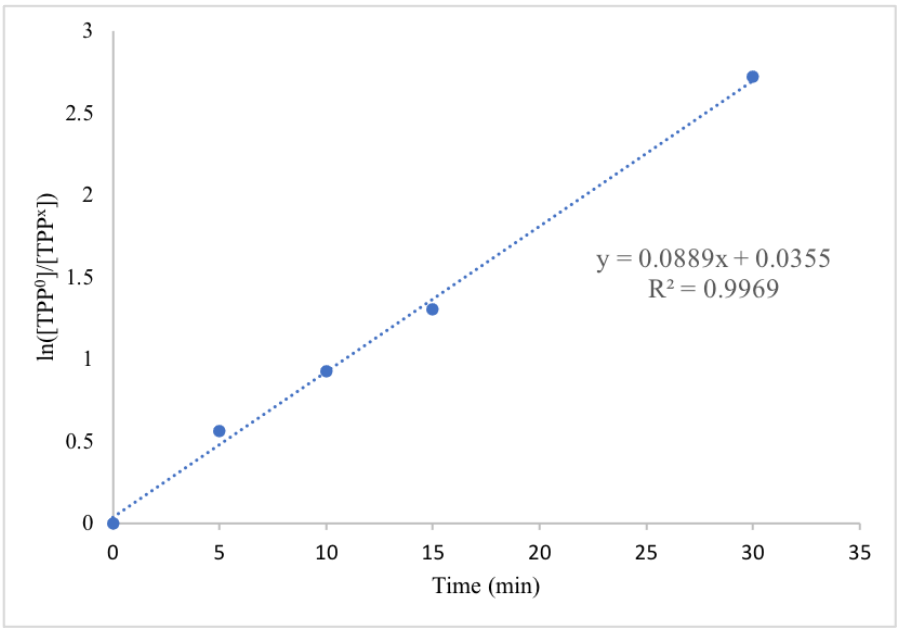


Figure 20: Graph of ln([TPP°]/[TPP*]) vs time (min)

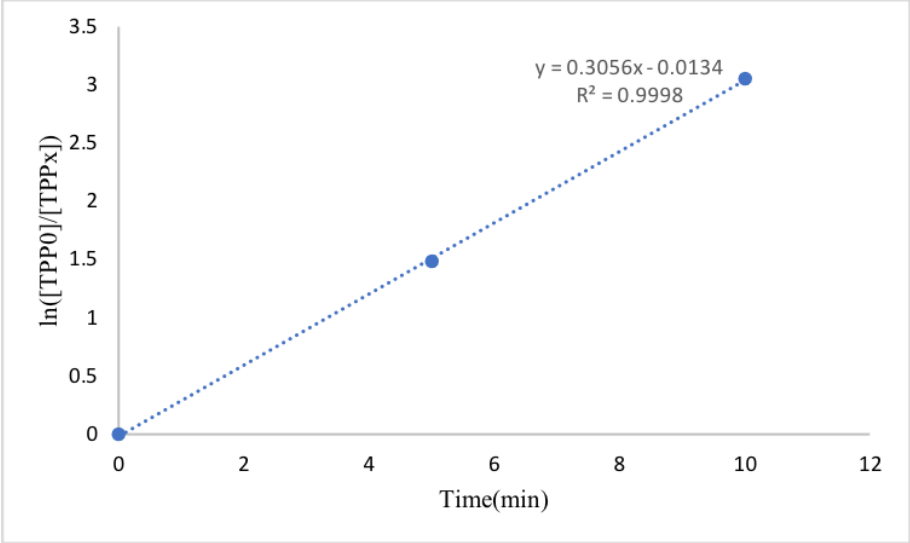


Figure 21: Graph of ln([DMA°]/[DMA*]) vs time(min)

CHAPTER 5

Concluding Remarks and Directions for Future Research

This study examined the photooxidation of arylphosphines within MOFs with porphyrin linkers. There was no change in the product distribution compared to the photooxidation of aryl phosphines in a homogeneous solution. Contrary to expectations, our findings suggest that singlet oxygen diffuses out of the MOF cages, and all photooxidation reactions occur in the solution phase. Furthermore, comparative studies with different MOFs showed that the Al-TCPP MOF reacts is a better photocatalyst for the photooxidation of aryl phosphines than TCPP.

We have also shown that ratios can be obtained for the first-order disappearance of various substrates in photooxidations catalyzed by MOFs. Comparing such ratios with the relative rate constant ratios from homogeneous solutions may indicate whether the reactions occur solely outside the MOF or inside and outside the MOF pores.

Future research directions should include studying the photooxidation of smaller molecules more likely to diffuse into the MOF pores to determine whether there is a rate enhancement relative to a homogenous solution using triphenylphosphine (which has no such enhancement) as a reference.

REFERENCES

(1) Derosa, M. C.; Crutchley, R. J. “Photosensitized singlet oxygen and its applications.” *Coord. Chem. Rev.* **2002**, *35*, 233-234.

(2) Greer, A. “Christopher Foote's Discovery of the Role of Singlet Oxygen [1O2 (1Δg)] in Photosensitized Oxidation Reactions.” *Acc. Chem. Res.* **2006**, *39*, 797-799.

(3) Durantini, A. M.; Greer, A. “Interparticle Delivery and Detection of Volatile Singlet Oxygen at Air/Solid Interfaces.” *Environ. Sci. Technol.* **2021**, *55*, 3559-3561.

(4) Baptista, M. S.; Cadet, J.; Di Mascio, P.; Ghogare, A. A.; Greer, A.; Hamblin, M. R.; Lorente, C.; Nunez, S. C.; Ribeiro, M. S.; Thomas, A. H.; Vignoni, M.; Yoshimura, T. M. “Type I and Type II Photosensitized Oxidation Reactions: Guidelines and Mechanistic Pathways.” *Photochem. Photobiol.* **2017**, *93*, 912-919.

(5) Mondal, S.; Jethwa, R. B.; Pant, B.; Hauschild, R.; Freunberger, S. A. “Singlet oxygen formation in non-aqueous oxygen redox chemistry: direct spectroscopic evidence for formation pathways and reliability of chemical probes.” *Faraday Discuss.* **2023**, *248*, 175-176.

(6) Zhang, D.; Ye, B.; Ho, D. G.; Gao, R.; Selke, M. “Chemistry of singlet oxygen with arylphosphines.” *Tetrahedron* **2006**, *62*, 10729-10733

(7) Castro-Olivares, R.; Günther, G.; Zanocco, A. L.; Lemp, E. Linear free energy relationship analysis of the solvent effect on singlet oxygen reactions with mono and disubstituted anthracene derivatives. *J. Photochem. Photobiol. A* **2009**, *207*, 160–166.

(8) Clennan, E. L.; Pace, A. “Advances in singlet oxygen chemistry *Tetrahedron* **2005**, 61, 6665.

(9) Ho, D.G.; Gao, R.; Celaje, J.; Chung, H.-Y.; Selke, M., “Phosphadioxirane: A Peroxide from an Ortho-Substituted Arylphosphine and Singlet Dioxygen,” *Science* **2003**, *302*, 259-262.

(10) Gao, R.; Ho, D. G.; Dong, T.; Khuu, D.; Franco, N.; Sezer, O.; Selke, M. Reaction of Arylphosphines with Singlet Oxygen: Intra- vs Intermolecular Oxidation. *Org. Lett.* **2001**, 3, 3719-3722.

(11) Zhang, D.; Celaje, J.; Agua, A.; Doan, C.; Stewart, T.; Bau, R.; Selke, M. "Photooxidation of Mixed Aryl and Biaryl Phosphines,” *Org. Lett.* **2010**, 10, 3100-3103

(12) Zhang, D.; Gao, R.; Afzal, S.; Vargas, M.; Sharma, S.; McCurdy, A.; Yousufuddin, M.; Stewart, T.; Bau, R.; Selke, M. “Intramolecular Arene Epoxidation by Phosphadioxiranes,” *Org. Lett.* **2006**, *8*, 5125-5128.

(13) Tolman, C.A. “Steric effects of phosphorus ligands in organometallic chemistry and homogeneous catalysis” *Chem. Rev.* **1977**, *77*, 313–348.

(14) Wang, X.; Lv, H.; Sun, Y.; Zu, G.; Zhang, X.; Song, Y.; Zhao, F.; Wang, J. “New porphyrin photosensitizers—Synthesis, singlet oxygen yield, photophysical properties and application in PDT.” *Spectrochimica Acta Part A: Molecular and Biomolecular Spectroscopy* **2022**, *279* DOI:10.1016/j.saa.2022.121447.

(15) Sreehari Surendran, R.; Xinlin, L.; Pravas, D. “Physical Properties of Porphyrin-Based Crystalline Metal-organic Frameworks.” *Commun. Chem.* **2021**, *4*, 47

(16) Liu, Y. “Metal-organic framework.” McGraw Hill’s Access Science. 2023. doi:10.1036/1097-8542.418633

(17) Fateeva, A.; Chater, P. A.; Ireland, C. P.; Tahir, A. A.; Khimyak, Y. Z.; Wiper, P. V.; Darwent, J. R.; Rosseinsky, M. J. "A Water-Stable Porphyrin-Based Metal-Organic Framework Active for Visible-Light Photocatalysis." *Angew. Chem. Int. Ed Engl.* **2012**, *51*, 7440–7444.

(18) Hao, Y.; Papazyan, E.; Ba, Y.; Liu, Y. "Mechanism-Guided Design of Metal-Organic Framework Composites for Selective Photooxidation of a Mustard Gas Simulant under Solvent-Free Conditions." *ACS Catal*. 2022, 12, 363−371.

(19) Wang, X.; Zhang, X.; Idrees, K. B.; Chen, Z.; Wu, Y.; Lee, S.; Cao, R.; Chen, Y.; Yang, L.; Son, F. A.; Islamoglu, T.; Peterson, G. W.; Mahle, J. J.; Farha, O. K. "Near-instantaneous catalytic hydrolysis of organophosphorus nerve agents with zirconium-based MOF/hydrogel composites." *Chem. Catal.* **2021**, *1*, 721-733

(20) Hao, Y.; Liu, B.M.; Bennett, T.F.; Monsour, C.G.; Selke, M.; Liu, Y. "Determination of Singlet Oxygen Quantum Yield of a Porphyrinic Metal-Organic Framework" *J. Phys. Chem. C* **2021**, *125*, 13, 7392–7400.

(21) Hemmer, K.; Cokoja, M.; Fischer, R. A. "Exploitation of Intrinsic Confinement Effects of MOFs in Catalysis." *Chem. Cat. Chem*. **2021**, *13*, 1683–1691.

(22) CSD-Mercury; Version 4.2.0; Cambridge Crystallographic Data Centre: Cambridge, UK (2019)

(23) J.P. Olivier. "Modeling Physical Adsorption on Porous and Nonporous Solids Using Density Functional Theory." *Journal of Porous Materials* **1995**, *3*, 9–17.